Statistical assessment of fatigue crack initiation from sub-surface hydrogen micropores in high-quality die-cast aluminum

Toda, Hiroyuki
Department of Mechanical Engineering, Toyohashi University of Technology

Masuda, Shortaro
Department of Mechanical Engineering, Toyohashi University of Technology

Batres, Rafael
Department of Mechanical Engineering, Toyohashi University of Technology

Kobayashi, Masakazu
Department of Mechanical Engineering, Toyohashi University of Technology

他

出版情報：Acta materialia. 59 (12), pp.4990-4998, 2011-07-01. Elsevier
バージョン：
権利関係：

Statistical assessment of fatigue crack initiation from sub-surface hydrogen micropores in high-quality die-cast aluminum

Hiroyuki Toda[a], Shotaro Masuda[a], Rafael Batres[a], Masakazu Kobayashi[a], Shunzo Aoyama[b], Masato Onodera[b], Ryosuke Furusawa[b], Kentaro Uesugi[c], Akihisa Takeuchi[c] and Yoshio Suzuki[c]

[a] Department of Mechanical Engineering, Toyohashi University of Technology, Toyohashi, Aichi 441-8580, Japan (e-mail: toda@me.tut.ac.jp, tel: +81-532446697, fax: +81-532446690 (H. Toda))

[b] Engineering Department, Ahresty Co., Nakahara 1-2, Mitsuya, Toyohashi, Aichi 441-3114, Japan

[c] Japan Synchrotron Radiation Research Institute, 1-1-1, Kouto, Mikazuki, Sayo, Hyogo 679-5198, Japan

Abstract

It has recently been discovered that micropores on the order of a few micron are agglomerated in high density in the sub-surface layer of aluminum alloys that have been produced in a high-quality die-casting process. It is known that fatigue behavior is dominated by the existence of the micropores. In the present study, geometrical parameters defining the relationship between fatigue crack initiation and micropores have been investigated using high-resolution X-ray microtomography, combined with two kinds of statistical analysis. It has been revealed that consideration of micropore pairs is necessary, and a number of parameters for paired micropores that may be

strongly associated with fatigue crack initiation have been extracted and statistically evaluated. It has been concluded that the mean diameter between paired micropores, and the mean distance to the casting surface, are predominant in fatigue crack initiation.

Keywords: X-ray tomography, fatigue crack initiation, in-situ observation, pore, Al-Si alloy

Introduction

The casting process inevitably introduces a variety of casting defects and defective microstructures detrimental to the mechanical properties of cast aluminum alloys. Well-known examples are porosity, intermetallic particles and entrapped oxide films. It has been well documented that these defects are especially deleterious to the fatigue behavior of cast aluminum alloys. One of the most detrimental defects in such alloys is porosity, which is caused by both shrinkage and precipitation of supersaturated hydrogen [1]. For example, it has been reported that fatigue cracks are initiated from porosity located at or near the specimen surface in 92 ~ 100 % of specimens in Al-Si alloys produced through various processes, such as gravity casting [2, 3], low-pressure permanent-mold die casting [4], and high-pressure die casting [5]. In addition, Li *et al*. have shown that the formation of fatigue cracks is dominated by the highest local stress–strain concentration caused by the presence of a pore adjacent to the free surface [6]. It has therefore been assumed that in cast aluminum alloys the time necessary for fatigue crack initiation can be substantially ignored, and almost all fatigue life is spent in crack propagation, even in the high-cycle-fatigue regime [7] that dominates crack initiation in other materials.

However, it can be readily imagined that this tendency is more or less dependent on pore size. For example, McDowell *et al*. have shown in their model analysis that incubation life (i.e., the time for both crack nucleation and propagation within the influence of a micro-notch root field) is about 50 ~ 70 % of the total life of 50 μm pores, but only about 20 ~ 30 % of the total life of 200 or 400 μm pores in the high-cycle-fatigue regime of an A356-T6 alloy [8]. Zhang *et al*. have examined the effects of the cooling rate during solidification on the fatigue life of a cast A356 aluminum alloy, and have concluded that when pore size is below a critical size of ~ 80 μm, due to a relatively high cooling rate during solidification, fatigue cracks are initiated from a near-surface eutectic microconstituent and not from pores [9].

Additionally, it has recently been discovered that micropores on the order of a few micron are agglomerated in high density in the sub-surface layer (typically within 20 ~ 30 μm from the casting surface) of aluminum alloys that have been produced in a high-quality die-casting process [10]. Although the size of such micropores is significantly smaller (4 ~ 5 μm on average) than the above-mentioned well-known casting defects, fatigue behavior was found to be dominated by the existence of the micropores. It has been reported that such micron-order-sized micropores are distributed in high density (approximately 8,000 pores/mm^3 in the above-mentioned high-quality die-cast aluminum alloy, and ~ 700,000 pores/mm^3 in standard aluminum alloys), except in pure aluminum [1, 10-12]. Since porosity is formed through the precipitation of supersaturated hydrogen, which is usually unavoidable due to the hydrogen solubility gap at the melting temperature of aluminum, it is physically impossible to completely eliminate micropores from aluminum alloys [11, 13]. It is reasonable to assume that a dominant fatigue crack is initiated from one or a few detrimental pores. Therefore, if the

geometrical nature of detrimental micropores can be directly related to fatigue crack-initiation behavior, it is expected that fatigue properties may be optimized by eliminating such detrimental pores. This technique would offer more effective and realistic microstructural control than one based on the evaluation of average pore size and/or pore population [14, 15].

This study reenacted the observation of fatigue crack initiation caused by micropores in a cast aluminum alloy, using high-resolution X-ray microtomography, an excellent technique that enables three-dimensional (3D) quantitative measurement, through in-situ observation, of all the microstructural features in a specimen, together with identification of micropores serving as fatigue crack initiators. .

2. Experiments

An AC4CH alloy, designated in the JIS standard, was employed in the experiments. The alloy had a chemical composition of 7.04 Si, 0.35 Mg, 0.115 Ti, 0.09 Fe, 0.008 Ni, 0.0065 Mn, 0.0025 Cu, and balance Al in mass %. Specimens were sampled from automotive components, so that the casting surface was preserved as one of the four specimen side surfaces. The components were cast using the New Injection (NI) process, and then tempered to a T6 temper condition with a solution heat-treatment for 18 ks at 803 K, followed by artificial ageing for 18 ks at 443 K. The NI process a low-speed mold-filling die-casting process in which air pressure is used to directly fill melting liquid into mold and to give pressure through plunger. Owing to low hydrogen content, casting can conduct heat treatment and welding. Two types of fatigue specimens were prepared; an ordinary plate specimen of 15 (length: L) × 5 (width: W) × 2 mm (thickness: B) and a parallelepiped specimen of 0.4 (L) × 0.6 (W) × 0.6 mm (B) in

gauge section with bonded end tabs for laboratory fatigue tests and in-situ observation under synchrotron radiation, respectively. All the specimen surfaces, other than the casting surface, were polished using a 1-μm-grade diamond abrasive.

Tension-to-tension fatigue tests were performed with a 49 N servo-hydraulic fatigue-testing machine at room temperature in air. Sinusoidal loading was applied with a load ratio, *R*, of 0.1, and a frequency of 30 Hz. In total, 40 specimens were prepared and tested at a maximum constant stress of 160 MPa. The casting surface had been removed in seven of the 40 by polishing, in order to investigate the effects of the surface condition. All the specimens were classified according to types in origin of the fracture. Variations in fatigue life were described using a two-parameter Weibull distribution function with mean ranking.

X-ray tomography was performed at the undulator beamline, BL47XU, of the SPring-8. An experimental hutch is located about 49 m from the X-ray source in this beam line. A monochromatic X-ray beam with a photon energy of 20 keV was used to observe the entire cross-section of the specimen and a region of about 622 μm in height. Image slices were reconstructed from a series of projections based on the conventional filtered back-projection algorithm. The gray value in each dataset was calibrated, unless otherwise noted, so that the linear absorption coefficient of -10 ~ 80 cm^{-1} fell in an 8-bit gray-scale range between 0 and 255. Isotropic voxels with 0.503 μm edges were achieved in the reconstructed slices. The threshold value for obtaining binary images was chosen as the median between the linear absorption coefficient peaks of air and the aluminum matrix. To suppress inaccuracies originating from image noise, only micropores over 23.168 voxels in volume were counted as micropores in the quantitative analysis. The other details of the tomography observation are available

elsewhere [1,11].

The in-situ loading stage [16] allowed specimens to be scanned under cyclic loading. Fatigue test conditions were identical to the laboratory fatigue tests except for the application, in this case, of a maximum constant stress of 130 MPa. In addition, the stress amplitude was reduced by about 19 % compared to the laboratory fatigue tests, in order not to overlook the instance of fatigue crack initiation. In total, 21 specimens were prepared and tested. A first tomographic scan was performed before loading in each specimen, and a second scan was performed after fatigue crack initiation was confirmed with radiographs. All the scans were performed while the specimens were subjected to a mean load under displacement control. To suppress the occurrence of blurring caused by the relaxation behavior of the material, the applied displacement was held for 20 min for aging before each scan.

3. Experimental results

3.1 Laboratory fatigue test results

The fatigue lives of the 40 specimens varied widely between 1.35×10^5 ~ 1.00×10^8 cycles. Note that one specimen had not been fractured, and the fatigue test for it was interrupted at 1.00×10^8 cycles. The mean fatigue lives for the specimens with and without casting surface were 5.71×10^6 and 3.93×10^7 cycles, respectively. This sevenfold difference may be explained in light of the origin-type of the fracture. Two fracture origin-types were observed for the specimens with casting surface. Of the 33 specimens with casting surface, three were fractured with surface scratch (typically 40 ~ 80 μm in depth) as the origin of the fracture, while in the remaining 30 specimens fatigue cracks were initiated by subsurface micropores, as shown in Fig. 1 (a). When

both surface scratch and micropores were identified on the fracture surface, it was classified as micropores, since fatigue crack initiation could be visually associated with the agglomerated micropores. In addition, the density of micropores was subjectively classified into three levels: high-density clustered micropores, high-density isolated micropores, and low density micropores (hereinafter HD (Clustered), HD (Isolated) and LD). The numbers of the three types were 7, 9 and 14, respectively. On the other hand, no distinct fracture origin was identified for the specimens without casting surface, which exhibited typical stage I crack growth in the subsurface region, as shown in Fig. 1 (b).

The scatter in fatigue life was statistically analyzed with the Weibull distribution function. Significant non-linearity was, however, observed when all the data was plotted together, suggesting the effects of multiple failure modes. All the data were therefore classified into five types according to the origins of the fracture: HD (Clustered), HD (Isolated), LD, surface scratch, and polished surface, as shown in Fig. 2. By classifying the data into these five types, the non-linearity in the Weibull plot was largely rectified. The value of the Weibull modulus was high when surface scratch and/or high-density micropores were observed, while relatively low Weibull moduli were obtained in the case of LD and polished surface. It is noteworthy that although there is an obvious difference between HD and LD, the effects of micropore agglomeration cannot be recognized in Fig. 2.

3.2 In-situ fatigue test results

Of the 21 specimens tested, no fatigue crack initiation was observed during fatigue loading of 250,000 cycles for 14 specimens. The fatigue tests of the 14

specimens were interrupted to make the most of a limited beam time for the synchrotron experiment. One to four fatigue cracks were observed between 80,000 ~ 230,000 cycles (111,428 cycles on average) in the remaining seven specimens. In total, 19,118 micropores were observed in the 21 specimens, as shown in Table 1. Only the micropores that are closest to the casting surface and not to the other polished surfaces were extracted in each specimen and statistically analyzed on fatigue crack initiation. The total number of micropores, porosity, and mean and maximum volume-equivalent pore diameters for all 21 specimens are listed in Table 1.

In specimen A, the initiation of a corner fatigue crack was confirmed at 230,000 cycles. Fatigue crack initiation and subsequent growth in the cuboidal region in specimen A is shown in Fig. 3; here, the four micropores from which the fatigue crack was initiated are highlighted in red, while the other micropores are shown in pink. One can see that the micropores are agglomerated in high density in the sub-surface layer. The air surrounding the specimen has been segmented and shown in gray to indicate the location of the casting surface, while the underlying aluminum has been removed in order to visualize the fatigue crack. It is interesting to note that the fatigue crack is not semicircular or quadrant-shaped, but elongated in parallel to the casting surface, suggesting that fatigue crack initiation due to the existence of the micropores occurs much more easily than fatigue crack growth.

In total, 50 micropores associated with fatigue crack initiation were identified in the seven specimens in which fatigue crack initiation was confirmed. The mean volume-equivalent pore diameter of the 50 micropores was 6.1 μm, which was 74 % larger than the overall average throughout the 21 specimens. It is reasonable to assume that both micropore size and distance to the casting surface are of crucial importance in

understanding fatigue crack-initiation behavior. The two parameters were plotted in Fig. 4 for the two types of micropores, those from which fatigue cracks were initiated, and those which remained intact. Although Fig. 4 suggests that fatigue cracks are prone to be initiated from relatively large pores, no clear correlation was obtained between fatigue crack initiation and the two parameters.

4. Statistical analysis of coarsened 3D data sets

4.1 Data coarsening method

In Section 3, it was shown that high-density micropores exert significant influence on fatigue crack initiation. The geometrical parameters of individual micropores could not, however, be strongly associated with fatigue crack initiation. It is reasonable to assume that since a fatigue crack is initiated from a location of high-tensile stress concentration in the subsurface layer, a limited number of micropores contribute to the fatigue crack initiation. For example, the stress elevation near a spherical cavity becomes 1 % at about 9.7 μm from a cavity center for the average micropore diameter of 3.1 μm, using the conventional equation for stress concentration [17]. The measured distance between each nearest-micropore pair was 6.8 μm on average, implying that only relatively near micropores should be taken into account when defining the relationship between micropores and fatigue crack initiation. There were 6,662 and 3,069 neighboring micropore pairs, with a mutual distance within 9.7 μm, in the 21 specimens and their regions of interest, respectively, as shown in Table 1.

It is reasonable to assume that since the shape of each micropore is almost spherical, as shown in Fig. 3, the geometrical parameters governing fatigue crack initiation from micropores would be the mutual distance and azimuth angle between

neighboring micropores, in addition to the micropore size and distance to the casting surface that have been evaluated in Fig. 4. Six parameters have been defined in order to express these geometrical features. Parameters x_1 and x_3 have been defined for each single micropore, while parameters x_2 and and x_4 ~ x_6 have been defined for micropore pair. Parameters x_1 and x_2 describe diameter of a single micro pore and mean diameter of paired micro pores, respectively. Parameters x_3 and x_4 describe distance to a casting surface for a single micro pore and paired micro pores, respectively. x_5 and x_6 are the distance between paired micro pores and the angle between a line connecting paired micro pores and the horizontal axis, respectively. These parameters have been calculated for all 21 specimens before statistical analysis, and have thereby been utilized as a form of data coarsening in this study. x_1 ~ x_6 have been normalized in advance to distribute between 0 ~ 1, in line with the following normal distribution function:

$$f(x) = y_0 + A\exp\left\{-\frac{1}{2}\left(\frac{x - x_c}{w}\right)^2\right\} \qquad (1)$$

where y_0, A, x_c and w are an offset value, amplitude, median value and full width at half maximum, respectively. The upper limit (a 99 % confidence interval) obtained from equation (1) was used to define unity (i.e., the maximum value) for each parameter, and each parameter was defined such that its value was larger when fatigue crack initiation was more apt to occur. For example, x_1 is a unity when the diameter of a single micropore is the largest, and x_5 is a unity when the average distance from two neighbouring micropores to the casting surface is the smallest. With respect to micropore diameter, since only micropores over 23.168 voxels in volume were treated

in this study, micropore diameters of less than this value are not inherently meaningful. A centering operation is therefore applied by subtracting 23.168 voxels in volume from every micropore diameter.

4.2 Test of independency for the geometrical parameters

The presence of independent variables associated with each other, which is called multicollinearity, inevitably causes decreased reliability and stability in multiple regression analysis, often leading to incorrect or confused understanding about relationships between independent and dependent variables [18]. Table 2 shows the correlation between each parameter pair as a form of contributing rate. The dependency between x_1 and x_2, and between x_3 and x_4, was obvious, whereas the contributing rates for the other combinations are one to three orders of magnitude smaller than the former two relationships. In such a situation, there are several ways to reduce the number of variables. In this study, a partial correlation coefficient, which can detect the marginal or partial contribution of a designated variable with the effects of the other variables being removed, was first applied, in order to avoid multicollinearity. Partial correlation coefficient values were calculated to be 0.0476, 0.1073, 0.0076, 0.0675, 0.0618 and 0.0711 for $x_1 \sim x_6$, respectively. Here, the first variable considered for removal was the one with the smallest partial correlation coefficient with respect to the dependent variable. In light of this, it was concluded that parameters x_1 and x_3 should be removed from the original six parameters. It is interesting to note that both of the removed parameters are associated with a single micropore, and that the four remaining parameters express the geometrical features of micropore pairs.

Before the statistical analysis, principal component analysis was employed to

assess the validity of the partial correlation coefficient analysis. Principal component analysis is a procedure for grouping variables so that each newly set group is mutually uncorrelated, by rotating original axes to new orientations that are orthogonal to each other [19]. The results of the principal component analysis are summarized in Fig. 5. The numbers represent the values of the projections of the original values of the parameters on the first two components. The arrows represent the eigenvectors of the covariance of the original variables, relating each parameter to each principal component. It can be clearly confirmed that parameters x_1 and x_2 and parameters x_3 and x_4 are respectively close in orientation, as has been concluded in the partial correlation coefficient analysis. The small angle between the vectors representing x_1 and x_2 implies that both parameters are highly correlated. The same may be said for the vectors representing x_3 and x_4, On the other hand, the opposite angles between x_5 and x_6 show the possibility of a negative correlation. Also, the almost parallel orientation of these last two parameters with respect to the vertical axis shows that x_5 and x_6 have high contributions to the second principal component. These assertions are notably stronger in regards to the correlation between x_1 and x_2, and between x_3 and x_4, because the equally long length of these vectors shows that the parameters are adequately represented by the first two principal components.

Classification and regression tree (CART) analysis was performed to investigate the importance of the parameters. CART is a non-parametric classification technique that is widely used for developing decision rules. The result of the CART analysis is shown in Fig. 6. The first three top nodes in the diagram corroborate the results of the principal component analysis. In other words, it would be possible to conclude the presence of fatigue crack parameters by at least knowing the values of x_2,

x_4, and x_5.

4.3 Results of the micropore-pair analysis

The parameters defined and selected in the preceding sections have been used to statistically describe the fatigue crack initiation behavior. Simple multi-regression analysis has been applied in the present study. Since no physical model has been proposed to date to describe the relationship between the geometrical features of micropore pairs and fatigue crack initiation, a simple multiple linear regression has been applied in order to estimate the predominant geometrical parameters:

$$y = a_0 + a_1x_1 + a_2x_2 + a_3x_3 + a_4x_4 + a_5x_5 + a_6x_6 \qquad (2)$$

where a_0 is an intercept, and a_1 ~ a_6 are partial regression coefficients. The dependent parameter is y = 1 when a micropore of interest causes fatigue crack initiation, and y = 0 when it is not associated with fatigue crack initiation. Multiple linear regression solves the latter function so that the squared deviations of the dependent variables from y are minimized. The partial regression coefficients have been estimated by means of the least squares estimation.

a_2, a_4, a_5 and a_6 were calculated for the selected four parameters to be 0.0580, 0.0567, 0.0221 and 0.0214, respectively. As has been discussed, the analysis based on the selected four parameters provided higher partial regression coefficients than that based on the six parameters (e.g., a_2 = 0.0455 and a_4 = 0.0510 in the six-parameter analysis). The partial regression coefficient for the mean diameter between paired micropores (a_2) is the highest, but not significantly different from that for the mean

distance from the paired micropores to the casting surface (a_4). On the other hand, the partial regression coefficients for the remaining two parameters, which express 3D alignment properties of the two micropores (a_5 and a_6), are roughly 40 % of those for the predominant parameters. The order of contribution to fatigue crack initiation is consistent with the results of the CART analysis.

4.4 Validation of the multiple regression analysis

This study has shown that the geometrical parameters predominant in fatigue crack initiation from micropores are micropore size and distance to the casting surface. For example, the importance of mean diameter may be visually confirmed in Fig. 7, where the predicted value, dependent variable and parameter x_2 of micropore size are plotted in 3D. It can be seen that both the predicted value and x_2 are relatively high for the micropores from which fatigue cracks were initiated, compared to those which remained intact. The predicted value increases with x_2, showing a strong correlation.

In order to verify the results of the multiple regression analysis of the substantive fatigue crack-initiation behavior, one specimen was picked up, and all the micropores in the vicinity of a fatigue crack were examined. Fig. 8 shows part of specimen B (40 μm (L) × 50 μm (W) × 155 μm (B)), in which micropores are agglomerated in relatively high density in a sub-surface layer, and a fatigue crack was confirmed just after initiation at 80,000 cycles. Forty micropores and 31 micropore pairs are located within the region shown in Fig. 8. Ten micropore pairs, which are highlighted in red, have been identified as fatigue crack initiators. The mean micropore size, and mean distance to the casting surface, of all the micropores shown in Fig. 8, which have been selected in the multiple regression analysis, are plotted in Fig. 9. The

statistically maximum micropore size and minimum distance to the casting surface for micropore pairs, which have been defined by the upper limit of 99 % confidence interval, are 5.4 μm and 1.8 μm on average, respectively. Five micropore pairs (P_1 ~ P_5), which are located in the middle of the fatigue crack, are larger than 5.4 μm in average diameter. All five micropore pairs served as fatigue crack initiators. When less than 5.4 μm on average, the distance to the casting surface for micropore pairs defines a border between fatigue crack initiation and no initiation. The boundary is located between 1.2 ~ 1.6 μm, which is close to the above minimum distance to the casting surface.

4.5 Interpretation of the multiple regression analysis

It has been well documented that there are significant surface effects on stress concentrations around a spherical cavity located in the vicinity of an object surface [20]. Given a micropore or micropore pair of 6.1 μm in diameter, located at 3.0 μm from the casting surface, and a mutual distance between the two pores of 3.0 μm (all of these being average values listed in Table 1), the maximum stress appears at pole A, and reaches about 2.2 times an applied stress [20], as shown schematically in Fig. 10. This multiplying factor increases rapidly with a decrease in the distance to the casting surface or an increase in micropore size. For example, when the distance to the casting surface decreases from 3.0 μm to 1.0 μm, the multiplying factor increases to about 2.7. It may be understood from Fig. 10 that when crack length, 2*a*, is 8 μm, the fatigue crack has almost passed through the stress field of the micropore in the case of the single micropore; while the majority of the crack front line is still being affected by the stress field of the two micropores in the case of the micropore pair, and it lasts until over 2*a* of 16 μm.

5. Summary

The fatigue life of an aluminum alloy produced in a high-quality die-casting process varies widely. High density micropores have recently been observed in the sub-surface layer of such an aluminum alloy. The statistical analysis of the scatter in fatigue life has revealed that the major fatigue crack initiator is micropores, and that the spatial distribution and density of the micropores are of crucial importance.

The observation of fatigue crack initiation from micropores has also been reenacted using high-resolution X-ray microtomography. In order to analyze the enormous quantity of volume data, six geometrical parameters have been used to extract geometrical information on the spatial distribution and density of micropores. Both single and paired micropores have been considered in the analysis. The presence of multicollinearity has been tested by investigating both partial correlation coefficients and principal components. Four parameters have been extracted in this way. The parameter extraction resulted in the removal of all the parameters for single micropores, while all the parameters for paired micropores remained. The results of the multiple regression analysis revealed that the mean diameter between paired micropores and the mean distance to the casting surface are predominant in fatigue crack initiation. It has been concluded that relatively proximate micropores should be especially taken into account, in order to better define relationships between micropores and fatigue crack initiation.

Acknowledgements

The support of the Light Metal Educational Foundation to HT is gratefully

acknowledged. The synchrotron radiation experiments were performed with the approval of JASRI through proposal numbers 2008A1142 and 2009A1289.

References

[1] Toda, H, Hidaka, T, Kobayashi, M, Uesugi, K, Takeuchi, A, Horikawa, K. Acta Mater. 57(2009), 2277-2290.

[2] Mo, D.F., He, G.Q., Hu, Z.F., Liu, X.S., Zhang, W.H., Mater. Sci. Engng. A, 527(2010), 3420-3426.

[3] Jang, Y, Jin, S, Jeong, Y, Kim, S, Metall. Mater. Trans. A, 40ª(2009), 1579-1587.

[4] Ammar, HR, Samuel, AM, Samuel, FH, Mater. Sci. Engng. A, 473(2008), 65-75.

[5] Mayer, H, Papakyriacou, Mm Zettl, B, Stanzl-Tschegg, SE, Int. J. Fatigue, 25(2003), 245-256.

[6] Li, P, Lee, PD, Maijer, DM, Lindley, TC, Acta Mater., 57(2009), 3539-3548.

[7] Wang, QG, Jones, PE, Metall. Mater. Trans. B, 38(2007), 615-621.

[8] McDowell, DL, Gall, K, Horstemeyer, MF, Fan, J, Engng. Fract. Mech., 70(2003), 49-80

[9] Zhang, B, Chen, W, Poirier, DR, Fatigue & Fracture of Engng. Mater. & Struct., 23(2000), 417-423.

[10] Masuda, S, Toda, H, Aoyama, S, Orii, S, Ueda, S, Kobayashi, M, J. Japan Foundry Engng. Soc., 81(2009), 312-319. (in Japanese)

[11] Toda, H, Minami, K, Koyama, K, Ichitani, K, Kobayashi, M, Uesugi, K, Suzuki, Y., Acta Mater., 57(2009), 4391-4403.

[12] Toda, H, Sinclair, I, Buffière, J.-Y., Maire, E, Khor, KH, Gregson, P, Kobayashi, T. Acta Mater., 52(2004), 1305-1317.

[13] Toda, H, Yamaguchi, T, Nakazawa, M, Aoki, Y, Uesugi, K, Suzuki, Y, Kobayashi, M, Mater. Trans., 51(2010), 1288-1295.

[14] Ting, J.C., Frederick, V., and Lawrence, F.V., Fatigue Fract. Eng. Mater. Struct., (16)1993, 631-647.

[15] Yi, J.Z., Gao, Y.X., Lee, P.D., Flower, H.M., and Lindley, T.C., Metall. Mater. Trans. A, 34A(2003), 1879-1890.

[16] Toda, H., Ohgaki, T., Uesugi, K., Kobayashi, M., Kuroda, N., Kobayashi, T., Niinomi, M., Akahori, T., Makii, K. and Aruga, Y., Metall. Mater. Trans. A, 37A(2006), 1211-1220.

[17] Edwards, R. H., ASME J. Appl. Mech., 19(1952), 19–30.

[18] Cohen, J. and Cohen, P., (1983). Applied Multiple Regression/Correlation Analyses for the Behavioral Sciences, Hillsdale, NJ: Lawrence Erlbaum Associates.

[19] Jolliffe, I. T. (1986). Principal Component Analysis. Springer-Verlag.

[20] Nishida, M. and Kim, P., Proc. 12th Japan Nat. Cong. Appl. Mech., (1963), 285-297.

Caption list

Fig. 1 SEM micrographs of fracture surface. Fracture surfaces have been classified into four types according to fatigue crack initiation sites. High density micropores are observed in (a), while no obvious defects are observed in the crack initiation site in (b).

Fig. 2 Weibull plots of fatigue lives tested at 160 MPa. Forty specimens have been tested in total, which have been classified into five types, according to the kind and level of the fatigue crack initiation site. The Weibull modulus is shown for each type in the figure.

Fig. 3 3D views of the fatigue crack initiation from micropores in the rectangular cuboid in specimen A. Note that one crack was initiated in the field of view. Micropores from which the fatigue crack has been initiated are highlighted in red. The air surrounding the specimen has been segmented and shown in gray, while the underlying aluminum has been removed in order to visualize the fatigue cracks.

Fig. 4 Relationship between the diameter of micropores and the distance to the casting surface. All the micropores contained in the 21 in-situ fatigue specimens are shown. Micropores from which fatigue cracks were initiated are shown in red.

Table 1 Results of the 3D image analysis of micropores contained in the 21 in-situ fatigue specimens. Micropores from which cracks were initiated have been analyzed separately.

Table 2 Summary of contribution rates, R^2, between each independent variable pair.

Fig. 5 Principal component score distribution of principal components 1 and 2. The arrows indicate eigenvectors.

Fig. 6 Schematic illustration of the tree-based model obtained using CART.

Fig. 7 Relationship between predicted value, Y_4, dependent variable, y, and independent variable, x_2.

Fig. 8 3D views of magnified fatigue crack initiation behavior in specimen B. Note that the fatigue crack has been initiated from the large micropore pairs located in the sub-surface region. The white lines indicate micropore pairs that have d_p larger than the statistical maximum value defined at 99 %.

Fig. 9 Relationship between the mean diameter of paired micropores, d_p and the mean distance to the casting surface, ℓ_p, for the micropores shown in Fig. 8. Micropore pairs from which the fatigue crack was initiated are shown in red.

Fig. 10 Schematic illustration of fatigue crack initiation from (a) a single pore, and (b) a micropore pair. Three different stages of fatigue crack growth (i.e., surface crack length, $2a$, of 0, 8 and 16 μm) are drawn.

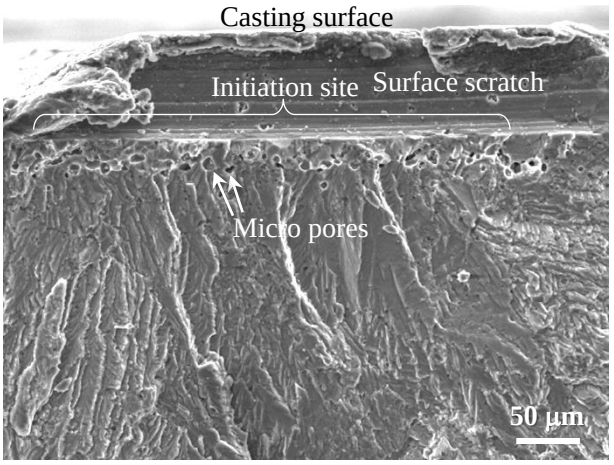

(a) High density pores : $N_f = 1.99 \times 10^5$

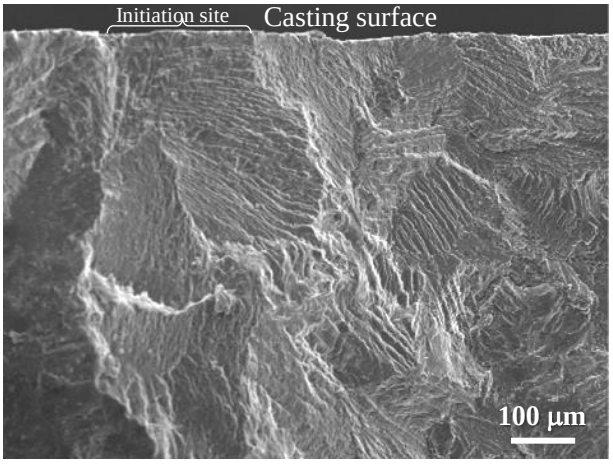

(b) No defects : $N_f = 2.47 \times 10^6$

Fig. 1 SEM micrographs of fracture surface. Fracture surfaces have been classified into four types according to fatigue crack initiation sites. High density micropores are observed in (a), while no obvious defects are observed in the crack initiation site in (b).

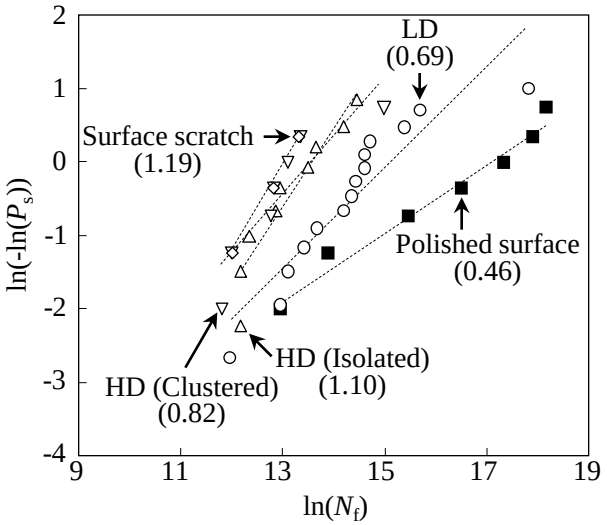

Fig. 2 Weibull plots of fatigue lives tested at 160 MPa. Forty specimens have been tested in total, which have been classified into five types, according to the kind and level of the fatigue crack initiation site. The Weibull modulus is shown for each type in the figure.

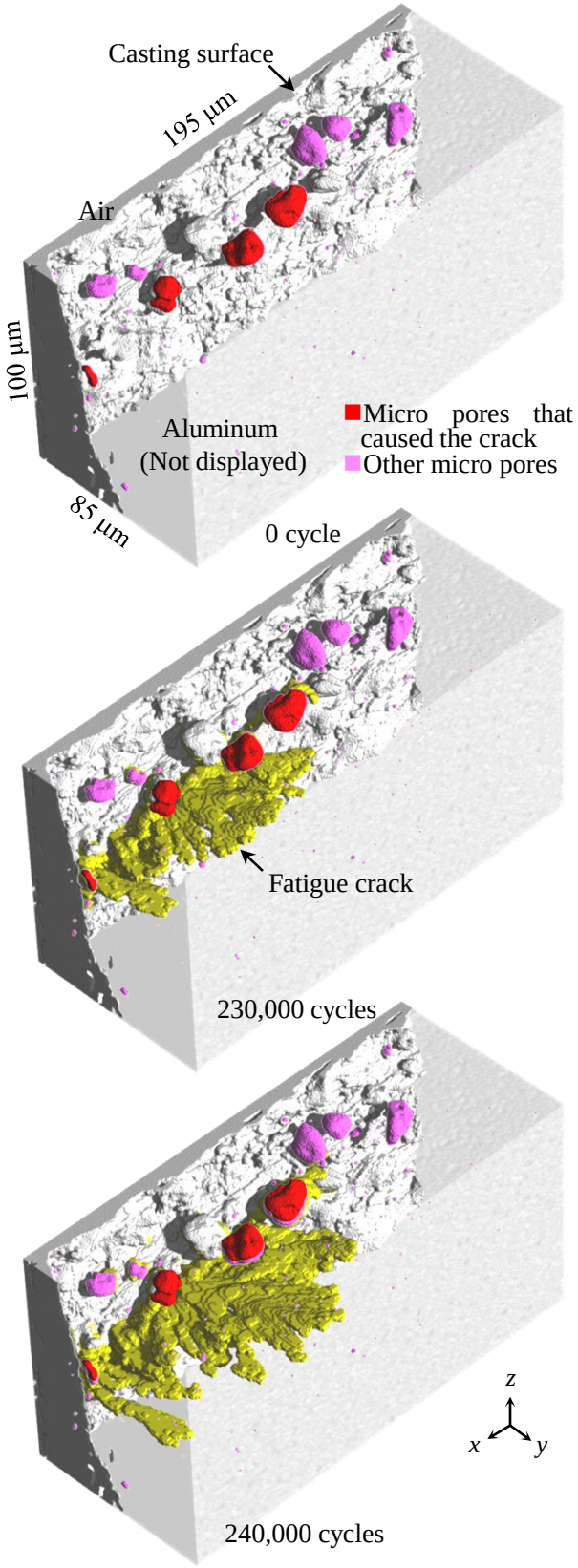

Fig. 3 3D views of the fatigue crack initiation from micropores in the rectangular cuboid in specimen A. Note that one crack was initiated in the field of view. Micropores from which the fatigue crack has been initiated are highlighted in red. The air surrounding the specimen has been segmented and shown in gray, while the underlying aluminum has been removed in order to visualize the fatigue cracks.

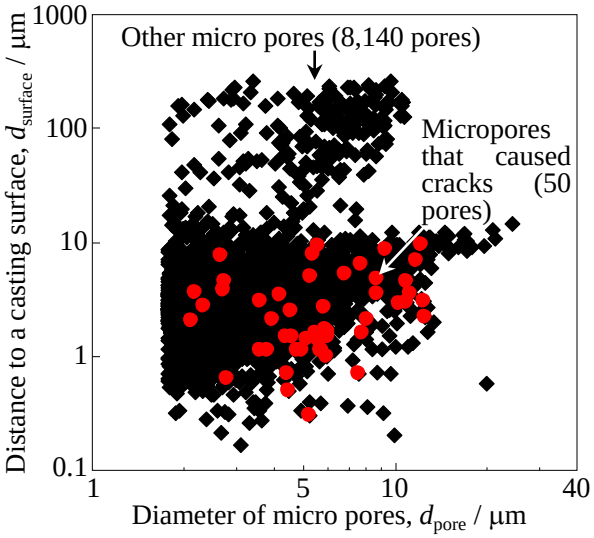

Fig. 4 Relationship between the diameter of micropores and the distance to the casting surface. All the micropores contained in the 21 in-situ fatigue specimens are shown. Micropores from which fatigue cracks were initiated are shown in red.

Table 1 Results of the 3D image analysis of micropores contained in the 21 in-situ fatigue specimens. Micropores from which cracks were initiated have been analyzed separately.

	Whole region	The region of interest analyzed*	Micro pores from which cracks are initiated
Number of specimens, n_{specimen}	21	21	7
Number of micro pores, n_{pore}	19118	8140	50
Number of micro pore pairs**, n_{pair}	6662	3069	22
Number density of micro pores, ρ / $\times 10^{12}$ m^{-3}	4.0	6.8	0.1
Volume fraction of micro pores, V_{f} (%)	0.014	0.035	0.003
Mean diameter of micro pores, $\bar{d}_{\mathrm{pore}}$ / μm	3.1	3.5	6.1
Maximum diameter of micro pores, $d_{\mathrm{pore}}^{\mathrm{max}}$ / μm	24.3	24.3	12.5
Mean distance to casting surface, $\bar{s}_{\mathrm{surface}}$ / μm	166.6	6.5	3.0
Mean distance between paired micro pores, $\bar{s}$ / μm	6.8	6.9	6.6

* The region in which only micropores closest to the casting surface exist.

** Micropore pairs defined as < 9.7 μm between gravity centers

Table 2 Summary of contribution rates, R^2, between each independent variable pair.

Independent variables	x_1	x_2	x_3	x_4	x_5	x_6
Diameter of a single micro pore, x_1	1	0.3898	0.0165	0.0109	0.0069	0.0001
Mean diameter of paired micro pores, x_2	0.3898	1	0.0291	0.0458	0.0292	0.0005
Distance to a casting surface, x_3	0.0165	0.0291	1	0.7484	0.0030	0.0019
Mean distance to a casting surface, x_4	0.0109	0.0458	0.7484	1	0.0015	0.0001
Distance between paired micro pores, x_5	0.0069	0.0292	0.0030	0.0015	1	0.0469
Angle to the horizontal axis, x_6	0.0001	0.0005	0.0019	0.0001	0.0469	1

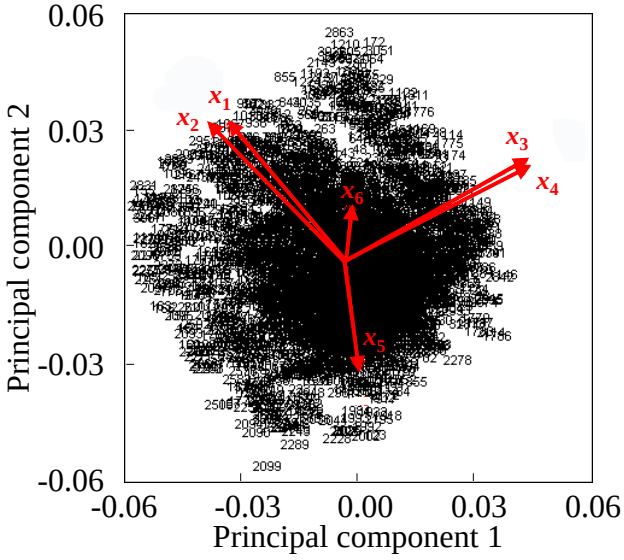

Fig. 5 Principal component score distribution of principal components 1 and 2. The arrows indicate eigenvectors.

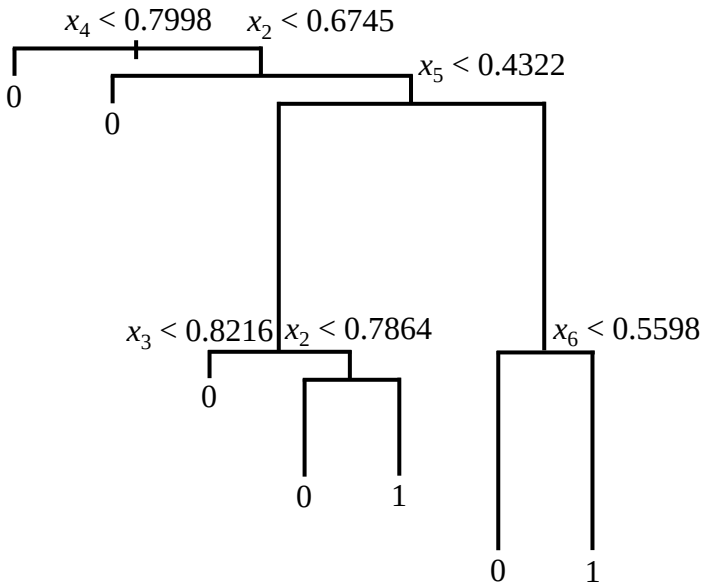

Fig. 6 Schematic illustration of the tree-based model obtained using CART.

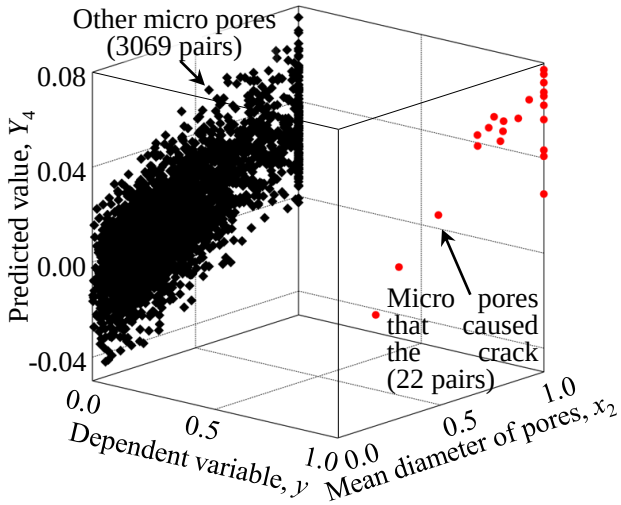

Fig. 7 Relationship between predicted value, Y_4, dependent variable, y, and independent variable, x_2.

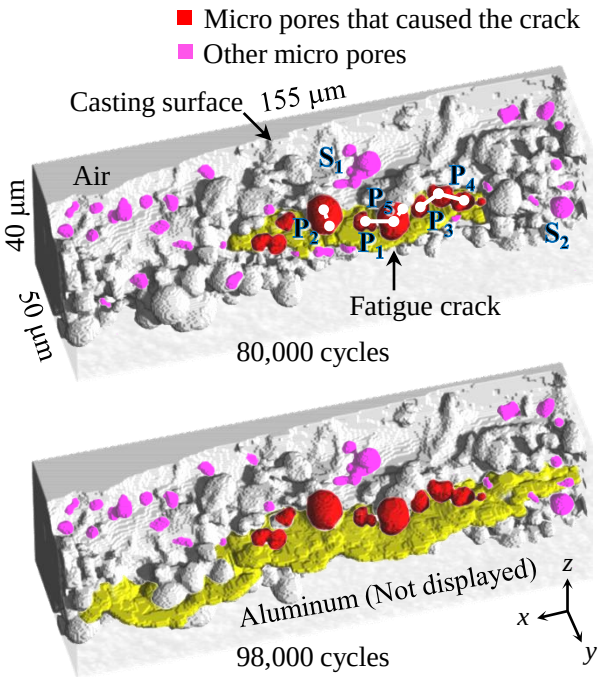

Fig. 8 3D views of magnified fatigue crack initiation behavior in specimen B. Note that the fatigue crack has been initiated from the large micropore pairs located in the sub-surface region. The white lines indicate micropore pairs that have dp larger than the statistical maximum value defined at 99 %.

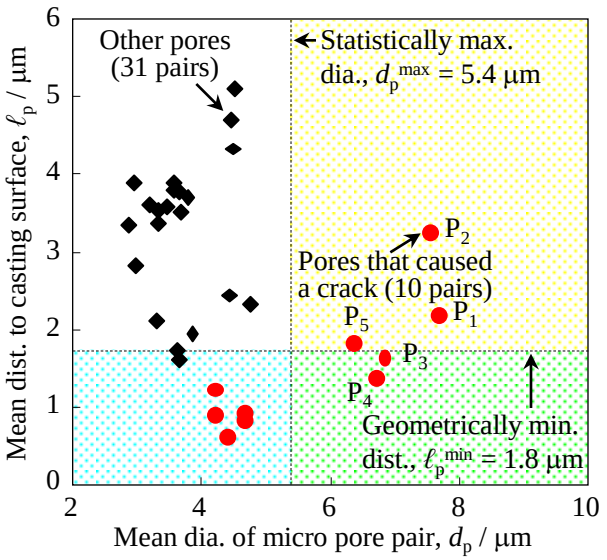

Fig. 9 Relationships between the mean diameter of paired micro pores, d_p and the mean distance to the casting surface, ℓ_p for the micro pores shown in Fig. 8. Micropore pairs from which the fatigue crack was initiated are shown in red.

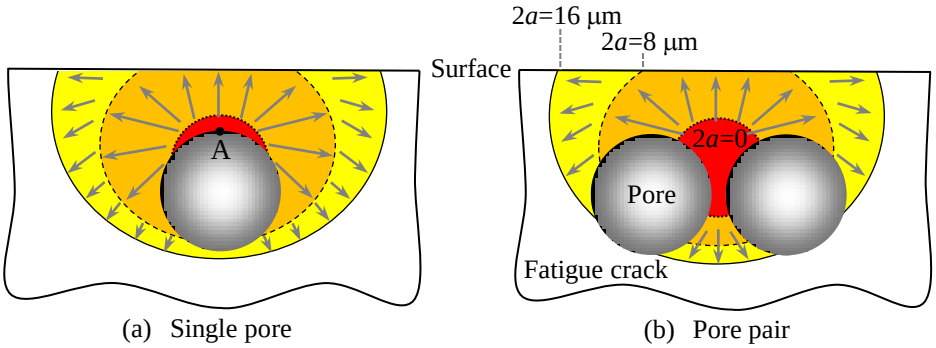

Fig. 10 Schematic illustration of fatigue crack initiation from (a) a single pore, and (b) a micro pore pair. Three different stages of fatigue crack growth (i.e., surface crack length, 2*a*, of 0, 8 and 16 μm) are drawn.